Extension of the Nonuniform Transformation Field Analysis using Tangent Second-Order expansion to nonlinear viscoelastic composites in the presence of aging and swelling

R. Largenton[a], J.-C. Michel[b], A. El Abdi[c], P. Suquet[b]

a. EDF-R&D, MMC, CEA Cadarache, Bât. 151, 13108 St Paul lez Durance Cedex,
rodrigue.largenton@edf.fr
b. Aix Marseille Univ, CNRS, Centrale Marseille, LMA UMR 7031, Marseille,
michel@lma.cnrs-mrs.fr, suquet@lma.cnrs-mrs.fr
c. CEA Cadarache, Bât. 151, 13108 St Paul lez Durance Cedex, akram.elabdi@cea.fr

Résumé :

Cette étude présente une modélisation micromécanique par le nouveau modèle NTFA-TSO du comportement viscoélastique d'un matériau hétérogène : un matériau composite triphasé composé de deux phases inclusionnaires dispersées dans une phase matrice. Les phases ont un comportement viscoélastique non linéaire vieillissant avec gonflement. L'approche par réduction de modèle est présentée dans un premier temps. Les champs locaux de variables internes sont décomposés sur une base réduite de modes et les potentiels de dissipation des phases sont remplacés par leur developpement tangent au second ordre. Les équations d'évolution réduites du modèle peuvent être entièrement exprimées à l'aide de quantités précalculées une fois pour toutes. Dans un deuxième temps, la précision du modèle NTFA-TSO développé est évaluée par comparaison à des simulations en champs complets.

Abstract:

This study presents a micromechanical modeling by the new NTFA-TSO model of the viscoelastic behavior of a heterogeneous material: a three-phase particulate composite material with two inclusion phases dispersed in a contiguous matrix. The phases have a nonlinear viscoelastic behavior with aging and swelling. First, the model-reduction approach is introduced. The local fields of internal variables are decomposed on a reduced basis of modes and the dissipation potentials of the phases are replaced by its tangent second-order expansion. The reduced evolution equations of the model can be entirely expressed in terms of quantities which are precomputed once for all. Second, the accuracy of the NTFA-TSO model is assessed by comparison with full-field simulations.

Keywords: Micromechanics, Model reduction, Nonlinear, Composite, Viscoelasticity, Aging, Swelling, Creep

1   Introduction

A common practice in multiscale problems for heterogeneous materials with well separated scales, is to look for homogenized, or effective, constitutive relations. In linear elasticity the structure of the homogenized constitutive relations is strictly preserved in the change of scales. The linear effective properties can be computed once for all by solving a finite number of unit-cell problems. Unfortunately there is no exact scale-decoupling in multiscale nonlinear problems which would allow one to solve only a few unit-cell problems and then use them subsequently at a larger scale. The response of representative volume elements along specific loading paths can be investigated numerically, but unfortunately these full-field simulations do not provide constitutive relations. Most of the huge body of information generated in the course of these costly computations is often lost.

Model-reduction techniques, such as the Nonuniform Transformation Field Analysis ([4]), may be used to exploit the information generated along such computations and, at the same time, to account for the commonly observed patterning of the local plastic strain field. A new version of the model was proposed in [5] (NTFA-TSO: Nonuniform Transformation Field Analysis using Tangent Second-Order expansion), with the aim of preserving the underlying variational structure of the constitutive relations (similar objective in [1]), while using approximations which are commonly used in nonlinear homogenization.

This study presents a micromechanical modeling by the new NTFA-TSO model [5] of the viscoelastic behavior of a heterogeneous material: a three-phase particulate composite material with two inclusion phases dispersed in a contiguous matrix. In an earlier study [2], the phases had an aging linear (one dissipation potential) viscoelastic behavior with swelling. The original NTFA [4] was applied in a three-dimensional setting and extended to account for inhomogeneous eigenstrains in the individual phases. In the present study, the phases have a nonlinear viscoelastic behavior with aging and swelling. The local dissipation potential is defined by the sum of two potentials, a quadratic potential corresponding to linear viscoelastic behavior and a non-quadratic power-law potential corresponding to nonlinear viscoelastic behavior. Due to the nonlinear dissipation potential within phases, the nonlinear procedure developed in [5] is required. First, the model-reduction approach is introduced. The local fields of internal variables are decomposed on a reduced basis of modes and the dissipation potentials of the phases are replaced by their tangent second-order expansion. The reduced evolution equations of the model can be entirely expressed in terms of quantities which are precomputed once for all. Second, the accuracy of the NTFA-TSO model is assessed by comparison with full-field simulations.

2   Three-phase particulate composite

We consider here a three-phase particulate composite already considered in [2] that has the following characteristics. The composite material is composed of two inclusion phases dispersed in a contiguous matrix phase. The first inclusion phase is the red phase and is referred to as the Pu clusters. Its volume fraction in the composite is 15% and the Pu clusters are assumed to be spherical with diameter varying in the range $[10\mu\text{m}, 70\mu\text{m}]$. The second inclusion phase is the blue phase and is referred to as the U clusters. Its volume fraction is 25% and the U clusters are assumed to be spherical with a constant diameter equal to $30\mu\text{m}$. The three-dimensional volume element considered is shown in Figure 1 and contains a total of 121 Pu clusters of different sizes and 57 U clusters (see [2] for more details on how this volume element was generated).
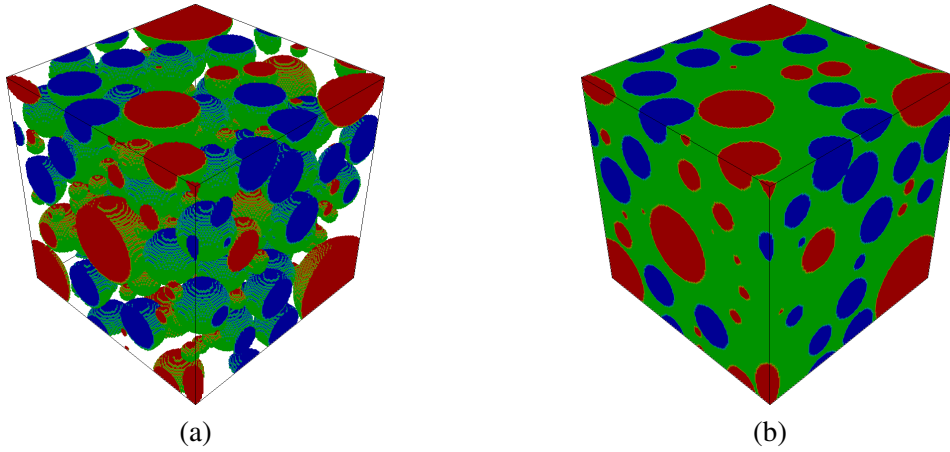
Figure 1: Three-dimensional volume element of the three-phase particulate composite. (**a**) Inclusions only - Pu clusters (in red), U clusters (blue). (**b**) Entire volume element - matrix (green).

3   Constitutive relations for the individual constituents

The composite material considered in this study is composed of individual constituents whose total strain can be decomposed into three contributions:

$$\boldsymbol{\varepsilon}(\boldsymbol{x},t) = \boldsymbol{\varepsilon}_{\mathsf{e}}(\boldsymbol{x},t) + \boldsymbol{\varepsilon}_{\mathsf{v}}(\boldsymbol{x},t) + \boldsymbol{\varepsilon}_{\mathsf{s}}(\boldsymbol{x},t), \tag{1}$$

where $\boldsymbol{\varepsilon}_{\mathsf{e}}$ is the elastic strain, $\boldsymbol{\varepsilon}_{\mathsf{v}}$ is the viscous strain and $\boldsymbol{\varepsilon}_{\mathsf{s}}$ is an eigenstrain of shrinkage-swelling. The elastic strain is related to the stress $\boldsymbol{\sigma}$ by the elastic compliance $\boldsymbol{M}$ (inverse of the elastic stiffness $\boldsymbol{L}$):

$$\boldsymbol{\varepsilon}_{\mathsf{e}}(\boldsymbol{x},t) = \boldsymbol{M}^{(r)} : \boldsymbol{\sigma}(\boldsymbol{x},t), \quad \boldsymbol{x} \text{ in phase } r. \tag{2}$$

The viscous strain rate derives from a dissipation potential ψ. ψ is defined by the sum of two potentials, a quadratic one, ψ_1, corresponding to a compressible linear viscoelastic behavior and a power-law second one, ψ_n, corresponding to a purely deviatoric nonlinear viscoelastic behavior:

$$\dot{\boldsymbol{\varepsilon}}_{\mathsf{v}}(\boldsymbol{x},t) = \frac{\partial \psi^{(r)}}{\partial \boldsymbol{\sigma}}(\boldsymbol{\sigma}(\boldsymbol{x},t)), \quad \boldsymbol{x} \text{ in phase } r, \quad \psi^{(r)}(\boldsymbol{\sigma}) = \psi_1^{(r)}(\sigma_{\mathsf{m}}, \sigma_{\mathsf{eq}}) + \psi_n^{(r)}(\sigma_{\mathsf{eq}}), \tag{3}$$

$$\psi_1^{(r)}(\sigma_{\mathsf{m}}, \sigma_{\mathsf{eq}})(\boldsymbol{x},t) = \frac{\sigma_{\mathsf{m}}^2(\boldsymbol{x},t)}{2k_{\mathsf{v}_1}^{(r)}} + \frac{\sigma_{\mathsf{eq}}^2(\boldsymbol{x},t)}{6G_{\mathsf{v}_1}^{(r)}(t)}, \quad \psi_n^{(r)}(\sigma_{\mathsf{eq}})(\boldsymbol{x},t) = \frac{\sigma_{\mathsf{eq}}^{n+1}(\boldsymbol{x},t)}{3(n+1)G_{\mathsf{v}_n}^{(r)}}, \tag{4}$$

where $\sigma_{\mathsf{m}} = \frac{1}{3}Tr(\boldsymbol{\sigma})$, $\sigma_{\mathsf{eq}} = \sqrt{\frac{3}{2}\boldsymbol{s}:\boldsymbol{s}}$ and $\boldsymbol{s}$ is the stress deviator. The time dependence of the shear viscosity modulus $G_{\mathsf{v}_1}^{(r)}(t)$ is due to aging and is shown in Figure 2**a** for each phase. The bulk viscosity modulus $k_{\mathsf{v}_1}^{(r)}$ and the shear viscosity modulus $G_{\mathsf{v}_n}^{(r)}$ can be assumed to be constant in time in each phase and their values are given in Table 1. Similarly, it is assumed that the elasticity of the phases is constant in time. In addition, the elasticity is assumed to be isotropic with the same moduli in each phase (see Table 1). The shrinkage-swelling strain is isotropic, uniform per phase and a function of time:

$$\boldsymbol{\varepsilon}_{\mathsf{s}}(\boldsymbol{x},t) = \varepsilon_{\mathsf{s}}^{(r)}(t)\,\boldsymbol{i}, \quad \boldsymbol{x} \text{ in phase } r, \tag{5}$$

where $\boldsymbol{i}$ is the second-order identity tensor. The evolution of $\varepsilon_{\mathsf{s}}^{(r)}(t)$ with time is shown in Figure 2**b**. It should be noted that the constitutive relations here defined have a generalized standard structure. The free energy w, from which the stress tensor $\boldsymbol{\sigma}$ derives, takes the form:

$$w(\varepsilon, \varepsilon_{\mathsf{v}}, \varepsilon_{\mathsf{s}}) = \frac{1}{2}(\varepsilon - \varepsilon_{\mathsf{v}} - \varepsilon_{\mathsf{s}}) : \boldsymbol{L} : (\varepsilon - \varepsilon_{\mathsf{v}} - \varepsilon_{\mathsf{s}}), \quad \boldsymbol{\sigma} = \frac{\partial w}{\partial \varepsilon}(\varepsilon, \varepsilon_{\mathsf{v}}, \varepsilon_{\mathsf{s}}). \tag{6}$$
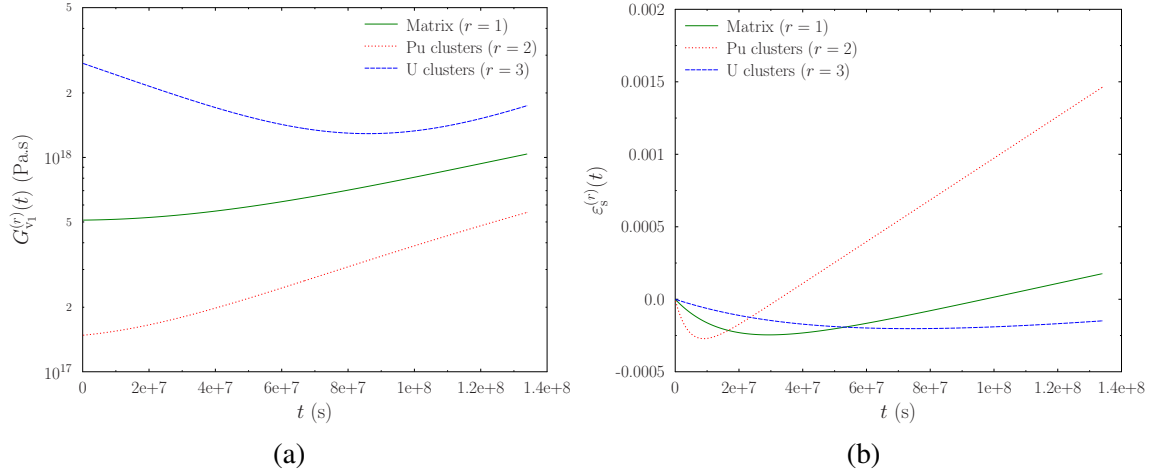

Figure 2: Evolution of $G_{\mathsf{v}_1}^{(r)}(t)$ (**a**) and $\varepsilon_{\mathsf{s}}^{(r)}(t)$ (**b**) with time for the three phases.

| Phase | E | ν | $k_{\mathsf{v}_1}^{(r)}$ | $G_{\mathsf{v}_n}^{(r)}$ | n |
	(Pa)	(-)	(Pa.s)	(Pa^n.s)	(-)
Matrix (r=1)	2.e+11	0.3	1.67e+18	1.e+39	3.67
Pu clusters (r=2)	2.e+11	0.3	5.01e+17	1.e+39	3.67
U clusters (r=3)	2.e+11	0.3	1.04e+19	1.e+39	3.67

Table 1: Material data for the individual constituents.

4 Exact local problem

A representative volume element V of the composite is comprised of N phases occupying domains $V^{(r)}$ with characteristic functions $\chi^{(r)}$ and volume fraction $c^{(r)}$. The spatial averaging over V and $V^{(r)}$ are denoted by $\langle . \rangle$ and $\langle . \rangle^{(r)}$ respectively. Periodic boundary conditions are assumed on the boundary ∂V of V. The loading is specified by imposing the macroscopic strain path $\overline{\varepsilon}(t)$ and the history of $\varepsilon_{\mathsf{s}}^{(r)}(t)$ in each phase. The exact local problem to be solved to determine the local stress and strain fields $\boldsymbol{\sigma}(\boldsymbol{x}, t)$ and $\varepsilon(\boldsymbol{x}, t)$ consists of the generalized thermoelastic problem (7), in which the field of internal variables $\varepsilon_{\mathsf{v}}(\boldsymbol{x}, t)$ is fixed,

$$\left.\begin{array}{c} \boldsymbol{\sigma}(\boldsymbol{x}, t) = \boldsymbol{L}(\boldsymbol{x}) : (\varepsilon(\boldsymbol{x}, t) - \varepsilon_{\mathsf{v}}(\boldsymbol{x}, t) - \varepsilon_{\mathsf{s}}(\boldsymbol{x}, t)), \\[2mm] \operatorname{div} \boldsymbol{\sigma}(\boldsymbol{x}, t) = 0, \quad \boldsymbol{\sigma}(\boldsymbol{x}, t) \cdot \boldsymbol{n}(\boldsymbol{x}) \text{ antiperiodic on } \partial V, \\[2mm] \varepsilon(\boldsymbol{x}, t) = \overline{\varepsilon}(t) + \frac{1}{2}(\boldsymbol{\nabla}\boldsymbol{u}^*(\boldsymbol{x}, t) + \boldsymbol{\nabla}\boldsymbol{u}^{*T}(\boldsymbol{x}, t)), \quad \boldsymbol{u}^*(\boldsymbol{x}, t) \text{ periodic on } \partial V, \end{array}\right\} \tag{7}$$

coupled with the differential equation (8) governing the evolution of the internal variables $\varepsilon_{\mathsf{v}}(\boldsymbol{x}, t)$ with time at every point $\boldsymbol{x}$ in V,

$$\dot{\varepsilon}_{\mathsf{v}}(\boldsymbol{x}, t) = \frac{\partial \psi}{\partial \boldsymbol{\sigma}}(\boldsymbol{x}, \boldsymbol{\sigma}(\boldsymbol{x}, t)), \tag{8}$$

where $\boldsymbol{L}(\boldsymbol{x}) = \sum_{r=1}^{N} \chi^{(r)}(\boldsymbol{x}) \boldsymbol{L}^{(r)}$ and $\psi(\boldsymbol{x}, \boldsymbol{\sigma}) = \sum_{r=1}^{N} \chi^{(r)}(\boldsymbol{x}) \psi^{(r)}(\boldsymbol{\sigma})$. The effective (or homogenized) constitutive relations relate the overall stress $\overline{\boldsymbol{\sigma}}(t)$ defined as the average of the local stress field

$$\overline{\boldsymbol{\sigma}}(t) = \langle \boldsymbol{\sigma}(\boldsymbol{x}, t) \rangle = \frac{1}{|V|} \int_V \boldsymbol{\sigma}(\boldsymbol{x}, t) \, d\boldsymbol{x},$$

to the history of the overall strain $\overline{\varepsilon}$ and of the shrinkage-swelling strains $\varepsilon_{\mathsf{s}}^{(r)}$.

5   The NTFA-TSO model

5.1   Nonuniform transformation fields

The basic feature of the NTFA theory [4] is a decomposition of the fields of internal variables on a finite set of predetermined shape functions (NTFA decomposition). This consists in writing in the present context:

$$\varepsilon_{\mathsf{v}}(\boldsymbol{x}, t) = \sum_{k=1}^{M} \xi^{(k)}(t) \, \boldsymbol{\mu}^{(k)}(\boldsymbol{x}), \tag{9}$$

where the fields $\boldsymbol{\mu}^{(k)}(\boldsymbol{x})$ are the *modes* and the $\xi^{(k)}$ are the *reduced internal variables*. The modes have the same tensorial character as the internal variables ε_{v}, so that the $\xi^{(k)}$ are scalar variables. To avoid a possible indeterminacy in the definition of the $\xi^{(k)}$, it is further assumed that the modes $\boldsymbol{\mu}^{(k)}$ are linearly independent fields. How the modes are chosen is discussed in section 6.1. The modes $\boldsymbol{\mu}^{(k)}(\boldsymbol{x})$ are assumed to be known in the following sections.

5.2   Macroscopic state laws and influence tensors

With the NTFA decomposition (9), the macroscopic state variables of the effective constitutive relations are the macroscopic strain $\overline{\varepsilon}(t)$ and the reduced internal variables $(\xi^{(k)}(t))_{k=1,\ldots,M}$. The local strain field $\varepsilon(\boldsymbol{x}, t)$ solution of the linear thermoelastic problem (7) with decompositions (9) and (5) can be expressed by superposition as:

$$\varepsilon(\boldsymbol{x}, t) = \boldsymbol{A}(\boldsymbol{x}) : \overline{\varepsilon}(t) + \sum_{k=1}^{M} (\boldsymbol{D} * \boldsymbol{\mu}^{(k)})(\boldsymbol{x}) \xi^{(k)}(t) + \sum_{r=1}^{N} (\boldsymbol{D} * \chi^{(r)} \boldsymbol{i})(\boldsymbol{x}) \varepsilon_{\mathsf{s}}^{(r)}(t), \tag{10}$$

where $\boldsymbol{A}(\boldsymbol{x})$ is the elastic strain localization tensor, $\boldsymbol{D}(\boldsymbol{x}, \boldsymbol{x}')$ is the nonlocal Green operator expressing the strain at point $\boldsymbol{x}$ resulting from a unit eigenstrain at point $\boldsymbol{x}'$ when the average strain vanishes and $*$ denotes the convolution in space. The elastic strain localization tensor $\boldsymbol{A}(\boldsymbol{x})$ and the influence tensors $(\boldsymbol{D} * \boldsymbol{\mu}^{(k)})_{k=1,\ldots,M}$, $(\boldsymbol{D} * \chi^{(r)} \boldsymbol{i})_{r=1,\ldots,N}$ can be computed once for all by solving $6 + M + N$ linear elasticity problems (see [2]). The corresponding stress field reads as:

$$\boldsymbol{\sigma}(\boldsymbol{x}, t) = \boldsymbol{L}(\boldsymbol{x}) : \boldsymbol{A}(\boldsymbol{x}) : \overline{\varepsilon}(t) + \sum_{k=1}^{M} \boldsymbol{\rho}^{(k)}(\boldsymbol{x}) \xi^{(k)}(t) + \sum_{r=1}^{N} \boldsymbol{\eta}^{(r)}(\boldsymbol{x}) \varepsilon_{\mathsf{s}}^{(r)}(t),$$

$$\boldsymbol{\rho}^{(k)}(\boldsymbol{x}) = \boldsymbol{L}(\boldsymbol{x}) : ((\boldsymbol{D} * \boldsymbol{\mu}^{(k)})(\boldsymbol{x}) - \boldsymbol{\mu}^{(k)}(\boldsymbol{x})), \quad \boldsymbol{\eta}^{(r)}(\boldsymbol{x}) = \boldsymbol{L}(\boldsymbol{x}) : ((\boldsymbol{D} * \chi^{(r)} \boldsymbol{i})(\boldsymbol{x}) - \chi^{(r)}(\boldsymbol{x}) \boldsymbol{i}).$$
$$\tag{11}$$

Knowing that the effective free energy $\widetilde{w}$ is the average in V of the local free energy w, the thermodynamic forces associated with the macroscopic state variables read:

$$\frac{\partial \widetilde{w}}{\partial \overline{\varepsilon}}(\overline{\varepsilon}, \boldsymbol{\xi}, \varepsilon_{\mathsf{s}}) = \overline{\boldsymbol{\sigma}} = \widetilde{\boldsymbol{L}} : \overline{\varepsilon} + \sum_{k=1}^{M} \langle \boldsymbol{\rho}^{(k)} \rangle \xi^{(k)} + \sum_{r=1}^{N} \langle \boldsymbol{\eta}^{(r)} \rangle \varepsilon_{\mathsf{s}}^{(r)},$$

$$-\frac{\partial \widetilde{w}}{\partial \xi^{(k)}}(\overline{\varepsilon}, \boldsymbol{\xi}, \varepsilon_{\mathsf{s}}) \stackrel{\text{def}}{=} \tau^{(k)} = \langle \boldsymbol{\mu}^{(k)} : \boldsymbol{\sigma} \rangle, \tag{12}$$

where $\widetilde{\boldsymbol{L}} = \langle \boldsymbol{L} : \boldsymbol{A} \rangle$ is the effective elastic stiffness tensor. Using (11), the reduced stress $\tau^{(k)}$ associated with the reduced internal variable $\xi^{(k)}$ can be expressed as:

$$\tau^{(k)}(t) = \boldsymbol{a}^{(k)} : \overline{\varepsilon}(t) + \sum_{\ell=1}^{M} D^{(k\ell)} \xi^{(\ell)}(t) + \sum_{r=1}^{N} H^{(kr)} \varepsilon_{\mathsf{s}}^{(r)}(t), \tag{13}$$

where the influence tensors $\boldsymbol{a}^{(k)}$, $D^{(k\ell)}$ and $H^{(kr)}$ are given by:

$$\boldsymbol{a}^{(k)} = \langle \boldsymbol{\mu}^{(k)} : (\boldsymbol{L} : \boldsymbol{A}) \rangle, \quad D^{(k\ell)} = \langle \boldsymbol{\mu}^{(k)} : \boldsymbol{\rho}^{(\ell)} \rangle, \quad H^{(kr)} = \langle \boldsymbol{\mu}^{(k)} : \boldsymbol{\eta}^{(r)} \rangle. \tag{14}$$

5.3 Complementary evolution laws – Tangent second-order linearization

Complementary evolution laws governing the evolution of the reduced internal variables $\xi^{(k)}$ need to be specified now. Fritzen and Leuschner [1] have proposed an hybrid formulation making use of the effective dissipation potential $\widetilde{\psi}$ defined by:

$$\widetilde{\psi} = \langle \psi(\boldsymbol{\sigma}) \rangle, \quad \boldsymbol{\sigma} \text{ given by (11)}. \tag{15}$$

As shown in [5] the definition (15) of the effective dissipation potential is not rigorously equivalent to the exact definition by duality but is a good approximation of it when the modes are rich enough. The evolution of the reduced internal variables $\xi^{(k)}$ is given by:

$$\dot{\xi}^{(k)} = \frac{\partial \widetilde{\psi}}{\partial \tau^{(k)}}. \tag{16}$$

(16) can be alternatively re-written as a differential equation for the reduced stresses $\tau^{(k)}$:

$$\dot{\tau}^{(k)} = \boldsymbol{a}^{(k)} : \dot{\overline{\varepsilon}} + \frac{\partial \widetilde{\psi}}{\partial \xi^{(k)}} + \sum_{r=1}^{N} H^{(kr)} \dot{\varepsilon}_{\mathsf{s}}^{(r)}. \tag{17}$$

At this point, it should be noted that the time integration of $\xi^{(k)}$ or $\tau^{(k)}$ requires the knowledge of the derivative of $\widetilde{\psi}$ with respect to $\tau^{(k)}$ or $\xi^{(k)}$ respectively. When the dissipation potential of the phases is non-quadratic, the knowledge of these derivatives requires the computation of local quantities before taking their average. This extra local step slows down considerably the method and has motivated an additional reduction by which all terms entering the time integration can be precomputed once for all ([5]). More precisely the tangent second-order linearization technique of Ponte Castañeda [6] is applied to the differential equation (17). In each phase r, the local potential $\psi^{(r)}$ is expanded to second-order

as:

$$
\psi^{(r)}(\boldsymbol{\sigma}) \simeq \psi_{TSO}^{(r)}(\boldsymbol{\sigma}) = \psi^{(r)}(\overline{\boldsymbol{\sigma}}^{(r)}) + \frac{\partial \psi^{(r)}}{\partial \boldsymbol{\sigma}}(\overline{\boldsymbol{\sigma}}^{(r)}) : \left(\boldsymbol{\sigma} - \overline{\boldsymbol{\sigma}}^{(r)} \right) +
$$
$$
\frac{1}{2} \left(\boldsymbol{\sigma} - \overline{\boldsymbol{\sigma}}^{(r)} \right) : \frac{\partial^2 \psi^{(r)}}{\partial \boldsymbol{\sigma}^2}(\overline{\boldsymbol{\sigma}}^{(r)}) : \left(\boldsymbol{\sigma} - \overline{\boldsymbol{\sigma}}^{(r)} \right),
\tag{18}
$$

where $\overline{\boldsymbol{\sigma}}^{(r)} = \langle \boldsymbol{\sigma} \rangle^{(r)}$, so that $\widetilde{\psi}$ is approximated by:

$$
\widetilde{\psi} \simeq \widetilde{\psi}_{TSO} = \sum_{r=1}^{N} c^{(r)} \left[\psi^{(r)}(\overline{\boldsymbol{\sigma}}^{(r)}) + \frac{1}{2} \frac{\partial^2 \psi^{(r)}}{\partial \boldsymbol{\sigma}^2}(\overline{\boldsymbol{\sigma}}^{(r)}) :: \boldsymbol{C}^{(r)}(\boldsymbol{\sigma}) \right],
$$
$$
\boldsymbol{C}^{(r)}(\boldsymbol{\sigma}) = \langle \left(\boldsymbol{\sigma} - \overline{\boldsymbol{\sigma}}^{(r)} \right) \otimes \left(\boldsymbol{\sigma} - \overline{\boldsymbol{\sigma}}^{(r)} \right) \rangle^{(r)}.
\tag{19}
$$

Using (19), (17) becomes:

$$
\dot{\tau}^{(k)} = \boldsymbol{a}^{(k)} : \dot{\overline{\boldsymbol{\varepsilon}}} + \sum_{r=1}^{N} c^{(r)} \left[\frac{\partial \psi^{(r)}}{\partial \boldsymbol{\sigma}}(\overline{\boldsymbol{\sigma}}^{(r)}) : \frac{\partial \overline{\boldsymbol{\sigma}}^{(r)}}{\partial \xi^{(k)}} + \frac{1}{2} \frac{\partial^2 \psi^{(r)}}{\partial \boldsymbol{\sigma}^2}(\overline{\boldsymbol{\sigma}}^{(r)}) :: \frac{\partial \boldsymbol{C}^{(r)}(\boldsymbol{\sigma})}{\partial \xi^{(k)}} + \right.
$$
$$
\left. \frac{1}{2} \frac{\partial^3 \psi^{(r)}}{\partial \boldsymbol{\sigma}^3}(\overline{\boldsymbol{\sigma}}^{(r)}) ::: \boldsymbol{C}^{(r)}(\boldsymbol{\sigma}) \otimes \frac{\partial \overline{\boldsymbol{\sigma}}^{(r)}}{\partial \xi^{(k)}} \right] + \sum_{r=1}^{N} H^{(kr)} \dot{\varepsilon}_{\mathsf{s}}^{(r)}.
\tag{20}
$$

With (11), as a result, the different terms entering the expansion of $\partial \widetilde{\psi} / \partial \xi^{(k)}$ can now all be expressed as functions of the variables $\overline{\boldsymbol{\varepsilon}}$, $\xi^{(\ell)}$ and $\varepsilon_{\mathsf{s}}^{(r)}$ with the help of precomputed quantities, depending only on the average and fluctuations per phase of the fields $\boldsymbol{L} : \boldsymbol{A}$, $\boldsymbol{\rho}^{(\ell)}$ and $\boldsymbol{\eta}^{(r)}$. In the case where the elastic stiffness tensor $\boldsymbol{L}$ is assumed to be homogeneous in all the volume element V (as it is the case here), only the average and the fluctuations per phase of the fields $\boldsymbol{\rho}^{(\ell)}$ and $\boldsymbol{\eta}^{(r)}$ are required. The differential equations (20) are integrated in time for a prescribed history of the macroscopic strain $\overline{\boldsymbol{\varepsilon}}(t)$ and of the shrinkage-swelling strains $\varepsilon_{\mathsf{s}}^{(r)}(t)$. This allows for the determination of the resulting history of the reduced stresses $\tau^{(k)}(t)$, then that of the reduced internal variables $\xi^{(k)}(t)$ by inverting the relations (13) and finally that of the macroscopic stress $\overline{\boldsymbol{\sigma}}(t)$ by means of (12)₁.

6   Assessment of the model

6.1   Modes

The choice of the modes $\boldsymbol{\mu}^{(k)}$ plays a key-role in the efficiency of the method. There is no universal choice for these modes and they should rather be chosen according to the type of loading which the structure is likely to be subjected to . For the case of interest here, the structure is subjected to a triaxial creep loading with shrinkage-swelling of the phases during time. The triaxiality of the macroscopic stress, as well as its intensity, depends strongly on the position in the structure. The selected modes $\boldsymbol{\mu}^{(k)}$ are from the following four elementary loadings:

- three uniaxial creep loadings with no shrinkage-swelling in the phases,

$$
i = 1, 2 \text{ or } 3, \quad \overline{\boldsymbol{\sigma}}(t) = \sigma \, \boldsymbol{e}_i \otimes \boldsymbol{e}_i, \quad \sigma = 100 \,\text{MPa}, \quad \varepsilon_{\mathsf{s}}^{(r)}(t) = 0 \text{ in each phase } r,
\tag{21}
$$

- one loading corresponding to a pure shrinkage-swelling of the phases with no macroscopic stress,

$$
\overline{\boldsymbol{\sigma}}(t) = \boldsymbol{0}, \quad \varepsilon_{\mathsf{s}}^{(r)}(t) \text{ as in Fig. 2b for each phase } r.
\tag{22}
$$

For each of these four loading cases, 25 snapshots of the viscous strain field are stored every 5.36×10^6 seconds of the full-field simulation. All the full-field simulations were performed using an in-house code based on a fast Fourier transform method for nonlinear constituents ([3]), the volume element shown in Figure 1 being discretized into 147^3 voxels. The actual modes are then extracted from snapshots by means of the Karhunen–Loève transform procedure (see for instance [2, 5] for more details). After application of this procedure, a total of 9 modes were selected (2 modes per uniaxial creep loading and 3 modes for the pure shrinkage-swelling test).

6.2   Effective response

A first check of the accuracy of the NTFA-TSO model can be performed at the macroscopic level by comparing the effective response of the composite as predicted by the model with full-field simulations. Four loading cases are considered. The first two correspond to the loading case (21) and (22) respectively. These two test cases are among the loadings used for the determination of the modes and the aim is first to check separately the accuracy of the tangent second-order linearization technique used to reduce the evolution equations (17). The other two test cases are defined as follows:

$$\overline{\boldsymbol{\sigma}}(t) = \sum_{i=1}^{3} \sigma_i \, \boldsymbol{e}_i \otimes \boldsymbol{e}_i, \quad \varepsilon_{\mathsf{s}}^{(r)}(t) \text{ as in Fig. } \mathbf{2b} \text{ for each phase } r, \tag{23}$$

with

$$\sigma_1 = -115 \text{ MPa}, \quad \sigma_2 = -115 \text{ MPa}, \quad \sigma_3 = -230 \text{ MPa}, \tag{24}$$

and

$$\sigma_1 = -10 \text{ MPa}, \quad \sigma_2 = -10 \text{ MPa}, \quad \sigma_3 = -6.66 \text{ MPa}, \tag{25}$$

respectively. These last two test cases were not used in the determination of the modes and the aim is now to check the accuracy of the NTFA-TSO model in its entirety for loading cases representative of the macroscopic stress state within the structure. (24) is representative of the macroscopic stress state at the center of the structure while (25) is representative of the one at the periphery. The effective response of the composite as predicted by the NTFA-TSO model is compared in Figure 3 with that obtained from full-field simulations for all the four loading cases. As can be seen, a very good agreement is found for all the four loading cases. The gain in computational time is shown in Table 2 for the test cases (24) and (25) representative of the fuel pellet loadings. In Fig. $\mathbf{3c}$ and $\mathbf{d}$ the stress direction $\boldsymbol{\Sigma}^0$ is defined as $\boldsymbol{\Sigma}^0 = \overline{\boldsymbol{\sigma}} / (\overline{\boldsymbol{\sigma}} : \overline{\boldsymbol{\sigma}})^{1/2}$.

	Full-field simulation (FFT)	NTFA-TSO model (CPU ratio = FFT/TSO)
Triaxial creep test (24)	10 146 s	1.92 s (CPU ratio = 5 284)
Triaxial creep test (25)	16 026 s	3.50 s (CPU ratio = 4 579)

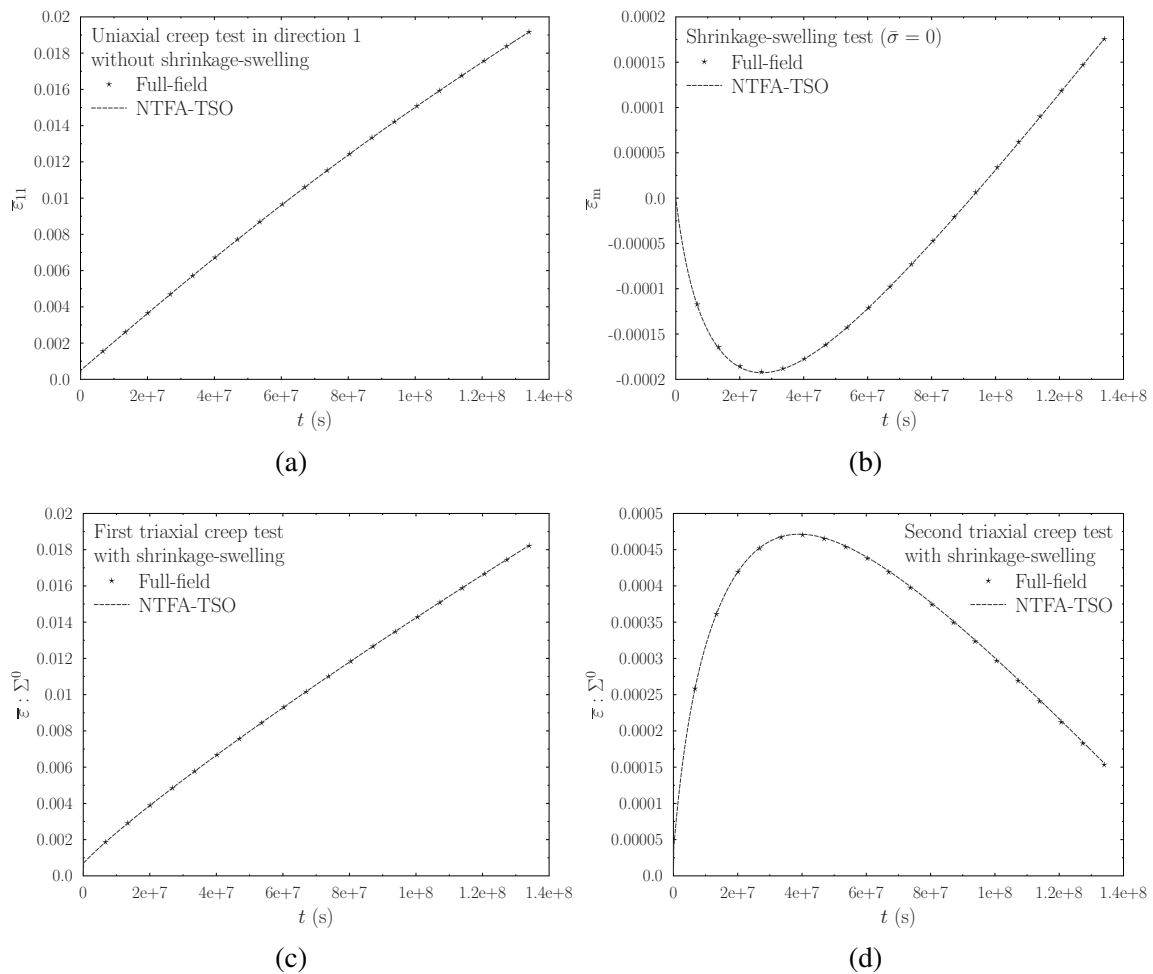Table 2: CPU times. Processor Intel Xeon X5687 @ 3.6 GHz.

Figure 3: Effective response. Comparison between full-field simulations (symbols) and the NTFA-TSO model (dashed line). (**a**) Uniaxial creep test in direction 1 without shrinkage-swelling in the phases. (**b**) Shrinkage-swelling test without macroscopic stress. (**c**) Triaxial creep test (24) with shrinkage-swelling in the phases. (**d**) Triaxial creep test (25) with shrinkage-swelling in the phases.

6.3 Local fields

A benefit of the NTFA method, already emphasized in [4, 2, 5], is that the local fields can be easily reconstructed from the knowledge of the reduced state variables and from pre-computed fields. This is in particular the case for the local strain field $\varepsilon(\boldsymbol{x}, t)$ of interest here which can be easily reconstructed by means of the relation (10). The probability density functions of the norm of the strain field in the three phases as predicted by the NTFA-TSO model and obtained by full-field simulations are compared in Figure 4 at the end of the test for the two triaxial creep loading cases (24) and (25) with shrinkage-swelling in the phases. The predictions of the NTFA-TSO model match quite well the full-field simulations in both the matrix phase and the U clusters, whereas the predicted distribution is a little shifted in the case of Pu clusters of different sizes.
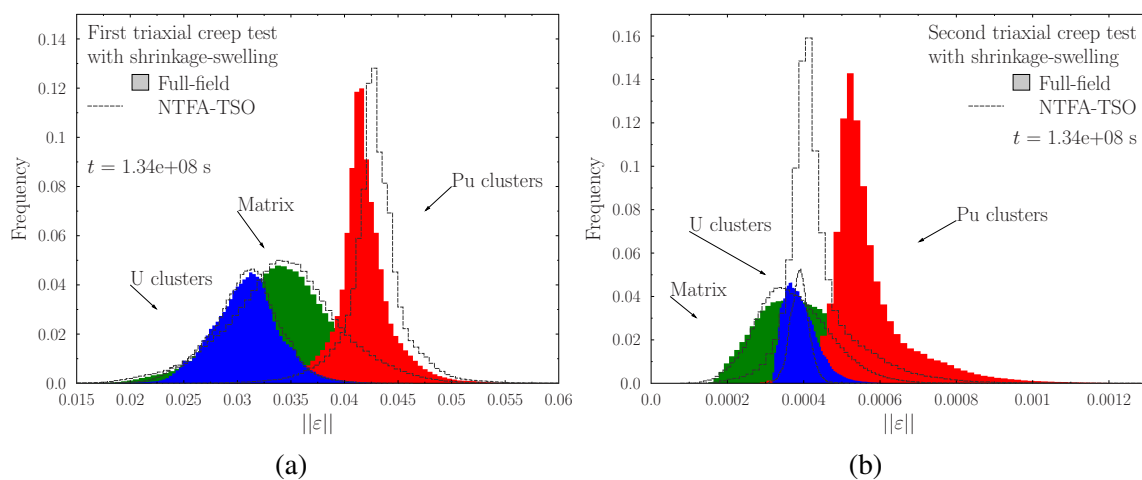
Figure 4: Probability distribution of the norm of the strain field in the different phases at the end of the test. Comparison between full-field simulations (full bars) and the NTFA-TSO model (dashed line). (**a**) Triaxial creep test (24) with shrinkage-swelling in the phases. (**b**) Triaxial creep test (25) with shrinkage-swelling in the phases.

7 Conclusion

The NTFA-TSO model has been extended to predict the nonlinear viscoelastic behavior of a three-phase composite material in the presence of aging and swelling. The accuracy of the model has been assessed by comparison with full-field simulations for triaxial creep loadings with shrinkage-swelling in the phases. The model predictions are in good agreement with the full-field simulations for the effective response of the composite as well as for the distribution of the local fields. The gain in computational time is more than three orders of magnitude.

References

[1] Fritzen F., Leuschner M., Reduced basis hybrid computational homogenization based on a mixed incremental formulation. Comput. Methods Appl. Mech. Engrg., 260 (2013) 143–154.

[2] Largenton R., Michel J.-C., Suquet P., Extension of the nonuniform transformation field analysis to linear viscoelastic composites in the presence of aging and swelling. Mechanics of Materials, 73 (2014) 76–100.

[3] Michel J.-C., Moulinec H., Suquet P., Effective properties of composite materials with periodic microstructure: a computational approach. Comput. Methods Appl. Mech. Engrg., 172 (1999) 109–143.

[4] Michel J.-C., Suquet P., Nonuniform transformation field analysis. Int. J. Solids Structures, 40 (2003) 6937–6955.

[5] Michel J.-C., Suquet P., A model-reduction approach in micromechanics of materials preserving the variational structure of constitutive relations. J. Mech. Phys. Solids, 90 (2016) 254–285.

[6] Ponte Castañeda, P., Exact second-order estimates for the effective mechanical properties of nonlinear composite materials. J. Mech. Phys. Solids, 44 (1996) 827–862.